1-1-2017

Effect of Pulse Shaping on Subharmonic Aided Pressure Estimation In Vitro and In Vivo.

Ipshita Gupta
Thomas Jefferson University, ipshita.gupta@jefferson.edu

John R. Eisenbrey
Thomas Jefferson University, john.eisenbrey@jefferson.edu

Maria Stanczak
Thomas Jefferson University, maria.stanczak@jefferson.edu

Anush Sridharan
Thomas Jefferson University; Drexel University, anush.sridharan@jefferson.edu

Jaydev K. Dave
Thomas Jefferson University, jaydev.dave@jefferson.edu

See next page for additional authors

Let us know how access to this document benefits you

Follow this and additional works at: https://jdc.jefferson.edu/radiologyfp

Part of the Radiology Commons

Authors

Ipshita Gupta, John R. Eisenbrey, Maria Stanczak, Anush Sridharan, Jaydev K. Dave, Ji-Bin Liu, Christopher Hazard, Xinghua Wang, Ping Wang, Huiwen Li, Kirk Wallace, and Flemming Forsberg

Effect of pulse shaping on subharmonic aided pressure estimation *in vitro* and *in vivo*

Ipshita Gupta[1,2], **John Eisenbrey**[1], **Maria Stanczak**[1], **Anush Sridharan**[1,3], **Jaydev K. Dave**[1], **Ji-Bin Liu**[1], **Christopher Hazard**[4], **Xinghua Wang**[5], **Ping Wang**[6], **Huiwen Li**[7], **Kirk Wallace**[4], and **Flemming Forsberg**[1]

[1]Department of Radiology, Thomas Jefferson University, Philadelphia, PA 19107, USA

[2]School of Biomedical Engineering, Sciences and Health Systems, Drexel University, Philadelphia, PA 19104, USA

[3]Department of Electrical and Computer Engineering, Drexel University, Philadelphia, PA 19104, USA

[4]GE Global Research, Niskayuna, NY 12309 ,USA

[5]Department of Ultrasound, The 2nd Hospital of Shanxi Medical University, Taiyuan, Shanxi 030001, China

[6]Department of Ultrasound, The Affiliated Hospital of North Sichuan Medical College, Nanchong, Sichuan 637000, China

[7]Department of Ultrasound, Erdos Center Hospital, Erdos, Inner Mongolia 017000, China

Abstract

Subharmonic imaging (SHI) is a technique that uses the nonlinear oscillations of microbubbles when exposed to ultrasound at high pressures transmitting at the fundamental frequency i.e., f_o and receiving at half the transmit frequency i.e., $f_o/2$. Subharmonic aided pressure estimation (SHAPE) is based on the inverse relationship between the subharmonic amplitude of the microbubbles and the ambient pressure change. Eight waveforms with different envelopes were optimized with respect to acoustic power at which the SHAPE study is most sensitive. The study was run with four input transmit cycles, first *in vitro* and then *in vivo* in three canines to select the waveform that achieved the best sensitivity for detecting changes in portal pressures using SHAPE. A Logiq 9 scanner with a 4C curvi-linear array was used to acquire 2.5 MHz radio-frequency data. Scanning was performed in dual imaging mode with B-mode imaging at 4 MHz and a SHI contrast mode transmitting at 2.5 MHz and receiving at 1.25 MHz. Sonazoid, which is a lipid stabilized gas filled bubble of perfluorobutane, was used as the contrast agent in this study. A linear decrease in subharmonic amplitude with increased pressure was observed for all waveforms (r from −0.77 to −0.93; p<0.001) *in vitro*. There was a significantly higher correlation of the SHAPE gradient with changing pressures for the broadband pulses as compared to the narrowband pulses in both *in vitro* and *in vivo* results. The highest correlation was achieved with a Gaussian

Corresponding Author Flemming Forsberg, PhD, FAIUM, FAIMBE Professor, Department of Radiology, 763H Main Building Thomas Jefferson University 132 South 10th Street Philadelphia, PA 19107, USA, tel: +1-215-955-4870, flemming.forsberg@jefferson.edu.

windowed binomial filtered square wave with an r-value of −0.95. One of the 3 canines was eliminated for technical reasons, while the other 2 produced very similar results to those obtained *in vitro* (r from −0.72 to −0.98; p<0.01). The most consistent *in vivo* results were achieved with the Gaussian windowed binomial filtered square wave (r = −0.95 and −0.96). In conclusion, using this waveform is an improvement to the existing SHAPE technique (where a square wave was used) and should make SHAPE more sensitive for noninvasively determining portal hypertension.

Keywords

Ultrasound; pulse envelope; subharmonic imaging; portal hypertension; noninvasive pressure estimation

---

Introduction

The long-term goal of this study is to develop a noninvasive technique for measuring portal hypertension using ultrasound with the aid of ultrasound contrast agents (UCAs). Portal hypertension is a condition resulting from obstruction of the portal blood flow. Cirrhosis, which is fibrosis of the liver due to many different etiologies including chronic alcohol abuse and hepatitis (1), is the most common cause of portal hypertension (2). Portal hypertension may also be caused by thrombosis i.e., a blood clot that develops in the portal vein. An increase of over 5 mmHg in the pressure gradient between the portal vein and the inferior vena cava or the hepatic vein is defined as portal hypertension (3).

Portal pressures are currently estimated using the hepatic venous pressure gradient (HVPG), which is defined as the difference between the wedged and free hepatic venous pressures (4).The current clinical technique for measuring HVPG is invasive and requires insertion of a balloon catheter via a transjugular approach into the hepatic vasculature. The wedged pressure is obtained by inflating the balloon thus, occluding the hepatic vein and is equivalent to the portal pressure, while the free pressure is measured with the catheter floating freely in the hepatic vein (4). An alternative accurate noninvasive ultrasound based procedure would be a major development in the diagnosis of portal hypertension making the diagnosis safer, quicker and less expensive.

UCAs are encapsulated microbubbles that oscillate nonlinearly within the pressure field caused by ultrasound pulses at higher incident pressures (> 200 kPa). The gas within these microbubbles has a different compressibility than blood leading to an acoustic impedance mismatch between the two, and an increase in scattering; hence, the microbubbles enhance the backscattered ultrasound signal (5). The UCA's nonlinear oscillations occur over a wide range of frequencies from subharmonics ($f_0/2$), and second harmonics ($2f_0$) to ultraharmonics ($3f_0/2$) of the insonation frequency as well as multiple thereof. These signals can be used to create contrast specific imaging modes, such as subharmonic imaging (SHI) as well as harmonic and superharmonic imaging (6). Harmonic imaging where ultrasound is transmitted at f_0 and received at $2f_0$ provides for restricted bandwidth since the tissue produces significant harmonic energy and leads to reduced blood to tissue contrast. SHI transmits at double the resonant frequency i.e., f_0 and receives at half the transmit frequency i.e., $f_0/2$ (6, 7). Since the surrounding tissue does not generate subharmonic response at the

low power levels used, SHI has an excellent contrast-to-tissue ratio i.e., the ratio of the mean bubble and tissue signal amplitudes. Contrast to tissue ratio values as high as 20 dB have been reported *in vitro* by Daechin et al. (8). Our group has proposed a novel and innovative technique called subharmonic-aided pressure estimation (SHAPE) (6, 9). It has been established previously that there are three stages in the subharmonic signal generation from microbubbles in response to changing acoustic pressure namely occurrence, growth and saturation (9). In the growth phase, the subharmonic signal amplitude has the highest sensitivity to pressure changes and an inverse linear relation with the ambient pressure (6, 9). It is this stage, which is used with the SHAPE procedure to estimate ambient pressure. An *in vitro* study comparing five different contrast agents showed Sonazoid (GE Healthcare, Oslo Norway), to be the most sensitive for SHAPE applications having the highest gradient in subharmonic amplitude as the pressure was changed from 0 to 186 mmHg and a correlation coefficient (r) of 0.99 (10).

The feasibility of using SHAPE to estimate the ambient pressures noninvasively has been confirmed by our group (9, 11, 12) and by others (13-15). High correlation coefficients have been reported (r= −0.98) in a static tank when pressure was varied from 0 to 186 mmHg with a slope of −0.07 dB/mmHg using a square enveloped input pulse (10). Another study analyzed the efficacy of SHAPE with Sonazoid in predicting portal hypertension in canines and showed r-values from −0.71 to −0.79 between the absolute portal vein pressure and subharmonic signal amplitude (16). A pilot study of SHAPE in 45 patients with chronic liver disease indicated SHAPE might become a useful tool for screening patients with portal hypertension and those at risk for variceal bleeding. The SHAPE gradient and HVPG values showed a linear correlation of 0.82 for subjects with a HVPG > 10 mmHg and 0.97 for patients with a HVPG > 12 mmHg (17).

Relatively little work has explored the effects of the pulse shape on the subharmonic response of microbubbles. Biagi et al. investigated the subharmonic response of Sonovue to different shaped pulses. They proved that the initial envelope of the pulse has a strong effect on the subharmonic amplitude (18). Zhang et al. showed that chirp excitation with a center frequency of 5 MHz enhances the subharmonic emission of encapsulated microbubbles (1). Another study by Shekhar and Doyley used rectangular windowed coded chirp excitation for intra vascular ultrasound imaging. They concluded that the chirp pulse with a higher bandwidth gave a 5.7 dB higher ratio of subharmonic to fundamental response amplitude than a narrowband sine wave. They also achieved a higher axial resolution with the broadband chirp pulse (19). In this study, eight waveforms with different envelopes were analyzed with respect to their ability to improve the SHAPE technique. These waveforms were selected to include different pulse envelopes based on various previous studies. The square wave was included as this is the traditional wave used for all our previous studies. Since chirp pulses showed increased subharmonic response in previous studies, they were included to test whether they improve the SHAPE sensitivity as well. All other pulses included had a varying degree of filtration of the square wave pulse to test for a different initial slope of the pulses. For each of the eight waveforms, the optimization algorithm previously developed by our group was run to select the optimum acoustic power (i.e., in the growth stage) (20). Scanning was then performed first *in vitro* and then *in vivo* in three

canines to select the waveform that provided the best correlation coefficient and had the best sensitivity for SHAPE portal hypertension measurements.

Materials and Methods

A set of eight pulse waveforms for SHI and SHAPE were tested in this study. The waveforms, along with their envelopes and alphabetical naming, are shown in fig.1. The square wave is the current pulse used in all the previous studies conducted by our group and is denoted as waveform A. A Logiq 9 scanner (GE Healthcare, Waukesha, WI, USA) with a 4C curvi-linear array was used to acquire radio-frequency data at the focal zone depth (9 cm) at a 12 Hz framerate. Scanning was performed in dual imaging mode with B mode operating at 4 MHz and contrast SHI transmitting 4 cycle pulses at 2.5 MHz and receiving at 1.25 MHz; based on our previous SHAPE studies (10, 16, 21-25). Data from each acquisition was saved as a DICOM file and the radio-frequency data extracted using proprietary software (GE Global Research, Niskayuna NY, USA). The extracted data gives both the B-mode and the subharmonic radio-frequency data, the latter of which is DC-filtered B mode data with a center frequency of 1.25 MHz and a 0.50 MHz bandwidth.

Additionally, the incident acoustic pressures from 0 to 100% were measured *in vitro* at the focus of the 4C transducer using a calibrated 0.5 mm needle hydrophone (Precision Acoustics, Dorchester, Dorset, UK; sensitivity of 337 mV/MPa at 2.5 MHz) using a standard water bath approach. The measured maximum incident acoustic pressures ranged from 1.0 to 1.6 MPa peak-to-peak.

In vitro Experimental Setup

Contrast signals at hydrostatic pressures varying from 10 to 40 mmHg were measured using a 2.25 L water tank. The water tank was also equipped with an acoustic window made out of thin plastic (thickness: 1.5 mm; Halldorsdottir *et al.*, 2011). The pressure inside could be varied by injecting air through a special inlet on the back wall of the tank and was monitored by a pressure gauge (OMEGA Engineering Inc., Stamford, CT, model DPG1000B-05G). An inlet on the top of the tank was constructed for injecting microbubbles and placing the pressure gauge. The scanner was used to acquire radio-frequency data at the optimized acoustic power associated with each individual waveform (in triplicate) for each pressure value following injection of the contrast in a 0.2 mL/L dose into saline (Isoton II; Coulter, Miami, FL). The mixture was kept homogenous by a magnetic stirrer. All data was acquired in triplicate.

In vivo Experimental Setup

All animal studies were approved by the Institutional Animal Care and Use Committee of our University and conducted in accordance with the guidelines provided by the NIH. A total of three canines were fasted for 24 hours to reduce portal vein flow and thus reduce experimental variability (26). The canines were kept under anesthesia during the entire procedure using standard techniques. The canines were placed on a warming blanket to maintain normal body temperature. Their abdomen was shaved and covered in gel to improve the acoustic interface to the transducer.

A midline abdominal incision was created to provide access to the main portal vein. An 18-gauge catheter was placed in a forelimb vein for contrast infusion. The pressure catheter (Millar Instruments, Inc., Houston, TX, USA) was connected to a digital oscilloscope (Model 9350 AM, LeCroy, Chestnut Ridge, NY, USA) through the transducer control unit (TCB 500, Millar Instruments) and then advanced through the splenic vein into the main portal vein to acquire pressure measurements simultaneously with the SHAPE study. The 4C probe was positioned transcutaneously over the portal vein. A sonographer with more than 10 years of experience performed all the scanning. A sonographer and a physician confirmed the presence of the pressure catheter in the portal vein and the patency of the portal vein using standard grayscale imaging.

An intravenous co- infusion of saline (120 ml/hour) and 0.18 mL/kg/hour of Sonazoid was employed based on prior experience (17, 27). All data was collected after visual verification of Sonazoid microbubbles in the portal vein.

The acoustic power was optimized independently for each of the 8 waveforms using the algorithm developed previously by our group (16). An region of interest within the portal vein was selected in the contrast image and the automated power control algorithm was initiated to determine the optimal acoustic output power for maximum SHAPE sensitivity to account for varying depth and attenuation. Briefly, the automated program acquires data for every acoustic output level, and the extracted subharmonic amplitude is plotted as a function of acoustic output. A logistic curve is fit to the data and the inflection point is selected as the optimized power, as this has been shown to be the point of greatest SHAPE sensitivity (9). One such curve is shown in figure 2.

Cine loops were collected in triplicate for 6 seconds, before and after induction of portal hypertension by embolization of the liver microcirculation. This was done through injection of approximatley 5 mL of Gelfoam (Ethicon, Somerville, NJ) mixed with 4 to 5 mL of saline (resulting in pressure values of 10 to 30 mmHg), into the main portal vein.

Data Processing and Analysis

The radio-frequency data from each acquisition was extracted using proprietary software (GE Global Research) as described above. Regions within the portal veins previously identified by the sonographer were selected on maximum intensity projection of B-mode images (compiled from reconstructed images from the radio-frequency data) and were fixed throughout the 6-second acquisition (approximately 27-30 frames). The subharmonic amplitude was calculated in a 0.5 MHz bandwidth around 1.25 MHz. Correlation coefficients and regression line slopes were calculated to check for the waveform with the best sensitivity and correlation with pressure. The waveform with the highest negative slope and a highly negative correlation coefficient (r) between the subharmonic amplitude and pressure was selected for further use in clinical trials. All statistical analysis was conducted using Matlab 2014b (The MathWorks, Inc, Natick, MA, USA). Waveforms were also divided into two groups of being broadband (waveforms B,E,F,G & H) and narrowband (waveforms A,C & D) and analyzed to determine if one group performed better than the other.

Results

In vitro

The *in vitro* tank data resulted in correlation values ranging from −0.77 to −0.95 between the subharmonic amplitude change and the hydrostatic pressure. All changes in subharmonic amplitude were statistically significant with increasing pressure (p<0.001). Fig.3 shows the reduction in subharmonic amplitude as the pressure is increased in the *in vitro* setup. The values for the correlation coefficients and the slope between the subharmonic amplitude and pressure change for all the eight waveforms are presented in Table 1.

Correlations were the highest for waveform E with an r value of −0.95 and a slope between the subharmonic amplitude and the hydrostatic pressure of −0.17 dB/mmHg. As can be seen from Table 1, the narrowband waveforms namely waveforms C and D had the lowest correlation coefficients and a smaller slope compared to the others. Hence, they were eliminated in the selection process for the best waveform.

In vivo

In the first canine, across all the eight waveforms, the normal baseline pressure was 9.9 ± 0.0 mmHg, which increased to 39.2 ± 0.4 mmHg post induction of hypertension. For the second canine, the baseline pressure was 9.4 ± 0.0 mmHg and it rose to 20.0 ± 0.8 mmHg post gelfoam injection. For the third canine, the baseline pressure was 11.2 ± 0.8 mmHg, which increased to 34.8 ± 1.6 mmHg post induction of hypertension.

Figure 4 shows a B mode and SHI image highlighting the portal vein and the pressure catheter along with the region of interest selection on its maximum intensity projection. The average signal over all the frames in the 0.5 MHz bandwidth around 1.25 MHz gave the subharmonic signal. The overall subharmonic amplitude in the third canine was much lower than in the other two (by about 12 dB) and too close to the noise floor to produce reasonable pressure estimates. This can be due to improper reconstitution of the agent. Hence, data from the third canine had to be excluded. The other two canines produced very similar results to those obtained *in vitro*. In the first canine, the pre-hypertension mean maximum subharmonic amplitude was 61.1 ± 2.00 dB which dropped to 47.7 ± 3.95 dB post the gelfoam injection for waveform E. Similar drops in the subharmonic amplitude for waveform E in the second canine were seen from a mean maximum subharmonic amplitude of 58.1 ± 1.14 dB to 44.8 ± 1.43 dB post the induction of hypertension. A reduction in subharmonic amplitude after the gelfoam injection was found to be statistically significant for all eight waveforms for the remaining two canines (p < 0.01).

For the first canine, the correlation coefficient for the group of broadband waveforms was −0.80 which was significantly better than the narrowband waveforms having a correlation coefficient of −0.63. Similar results were seen for the second canine where the broadband group had a significantly better correlation of −0.83 as compared to the narrowband group having an r value of −0.32, (p<0.05). No waveform was significantly better than the other within the broadband group (p>0.05).

However, in the first canine, within the broadband group, waveform E had the highest gradient of −0.44 dB/mmHg with a r value of −0.95. Waveform G and H had a lower slope as compared to the others with G having the lowest correlation of −0.72. The values are given in Table 2.

For the second canine again, waveform E had the best correlation with an r value of −0.96. It also had a steep negative slope. Waveforms G and H, even though showed a steep slope had a lower correlation than E and also didn't perform well consistently *in vitro* and in the first canine.

Waveform B performed well *in vitro,* however it did not perform well in either of the canines and hence, was discarded for further studies. Waveform H did not perform well in the *in vitro* analysis however, since it showed a high gradient with good linear regression in both the canines, to select the better waveform between E and H, the standard deviation between their slopes in both the canines was calculated. It was 0.01 dB/mmHg for waveform E and 0.13 dB/mmHg for waveform H. Also, waveform H had a lower slope than E in the first canine and did not achieve a correlation as good as E for the second canine. Since E had a smaller deviation in slope and was consistent with a highly negative slope and correlation, it was selected as the better waveform for SHAPE.

Discussion

The aim of this study was to assess the effect of eight different pulses on the sensitivity of SHAPE. Previous studies by Zhang et al. showed chirp signals with a center frequency of 5 MHz giving better subharmonic images with an increase of 22 dB in the subharmonic amplitude (1). Also, Maresca et al. studied the use of chirp excitation in intravascular ultrasound imaging *in vitro* with Definity as the UCA and compared it to conventional Gaussian shaped pulses. They observed a 9 dB increase in the signal-to-noise ratio when using the chirp pulse with a contrast-to-tissue ratio (Contrast to tissue ratio) of 12 dB (28).

Our group has previously used a square wave (which is waveform A for this study having a r value of −0.88) and reported a correlation coefficient between the subharmonic amplitude and ambient pressure of −0.98 in a static tank when pressure was varied from 0 to 186 mmHg with a slope of −0.07 dB/mmHg between the subharmonic amplitude and ambient pressure change (10). We were able to achieve an r value of −0.95 for the Gaussian windowed binomial filtered square wave (E) with a slope of −0.17dB/mmHg *in vitro. In vivo* with waveform E, the first canine had an r value −0.95 and a slope of −0.44 dB/mmHg; the second canine had an r value of −0.96 and a slope of −0.46 dB/mmHg. These values are higher than the previous studies with a square wave in canines where the r values ranged from −0.73 to −0.79 (16). The higher slopes and better correlation achieved in this study can be attributed to the automated power optimization and the effect of the different pulse envelopes used. That the pulse envelope has an effect on the subharmonic response has been proved by several studies. Shekhar and Doyley (19) concluded that chirp pulses with a higher bandwidth gave a 5.7 dB higher ratio of subharmonic to fundamental response amplitude than a narrowband sine wave. Our results are consistent with this. There was a significantly higher correlation of the SHAPE gradient with changing pressures for the

broadband pulses as compared to the narrowband pulses in both *in vitro* and *in vivo* results. Biagi and colleagues used SonoVue microbubbles and tested for the subharmonic amplitude of a 7.5 MHz sinusoidal burst signal as a reference wave against a Gaussian shaped pulse. They also tested a composite pulse (80 cycles of 5 MHz + 5 cycles of 2.5 MHz) against a reference sinusoidal pulse at 5 MHz. They found that the rectangular envelope reference pulse had a higher subharmonic amplitude in both settings and concluded that the steepness of the initial envelope greatly affects the subharmonic response of the UCAs (18). Zhang et al. showed that a rectangular envelope is effective in improving the subharmonic response by almost 35 dB than the Gaussian envelope (1). Similarly Daechin and co-workers also found that the subharmonic amplitude increases by up to 22 dB by changing the envelope from Gaussian to rectangular (29). In our study, waveform A which is a square wave (having a rectangular envelope) had a high SHI amplitude, but a relatively lower sensitivity to hydrostatic pressure. Waveform E, which is a Gaussian windowed binomial filtered version of the square wave, had a much greater slope with a highly negative correlation coefficient indicating that envelope is the most sensitive for SHAPE.

While the results are promising, there are certain limitations to this study. As discussed earlier, eight pulse sequences were tested in this study, since the scanner permits only eight pulse envelopes to be stored at a time. The results of the *in vivo* studies are based on a small sample size of three canines out of which one had to be excluded due to limited contrast enhancement. A larger sample size would increase the statistical power of the *in vivo* study.

Our group recently completed a pilot study of SHAPE in 45 patients with chronic liver disease, which indicated that SHAPE could become a useful tool for screening patients with portal hypertension and, in particular, those at risk for variceal bleeding. The SHAPE and HVPG values showed a linear correlation of 0.82 for all subjects and 0.97 for patients with a HVPG greater 12 mmHg (17). That study used a square wave. If the improved results with the new waveform are reproducible in a larger patient population, it may be possible to noninvasively and more accurately diagnose portal hypertension using SHAPE.

Conclusions

Eight waveforms were analyzed for SHAPE, both *in vitro* and *in vivo*. A significant reduction in the subharmonic amplitude was seen with increasing hydrostatic pressure for all eight waveforms. Results indicate that broadband pulses are more sensitive to the SHAPE estimations and a Gaussian windowed binomial filtered square wave (waveform E) gives the highest correlation between changes in subharmonic amplitude of the microbubbles and ambient pressure changes. Using this waveform is an improvement to the existing SHAPE technique and should make SHAPE more sensitive to non-invasively determining portal hypertension in the clinic.

Acknowledgements

References

1. Zhang D, Gong Y, Gong X, et al. Enhancement of subharmonic emission from encapsulated microbubbles by using a chirp excitation technique. Physics in Medicine and Biology. 2007; 52(18): 5531–44. [PubMed: 17804880]

2. Navarro, VJRS.; Herrine, SK. Pharmacology and Therapeutics: Principles to Practice. Saunders-Elsevier; 2008. Hepatic Cirrhosis.; p. 505-26.

3. Sanyal AJ, Bosch J, Blei A, Arroyo V. Portal hypertension and its complications. Gastroenterology. 2008; 134(6):1715–28. [PubMed: 18471549]

4. De Franchis R, Dell'Era A. Invasive and Noninvasive Methods to Diagnose Portal Hypertension and Esophageal Varices. Clinics in Liver Disease. 2014; 18(2):293–+. [PubMed: 24679495]

5. Stride EP, Coussios CC. Cavitation and contrast: the use of bubbles in ultrasound imaging and therapy. Proceedings of the Institution of Mechanical Engineers Part H-Journal of Engineering in Medicine. 2010; 224(H2):171–91.

6. Forsberg F, Liu JB, Shi WT, et al. In vivo pressure estimation using subharmonic contrast microbubble signals: Proof of concept. Ieee Transactions on Ultrasonics Ferroelectrics and Frequency Control. 2005; 52(4):581–3.

7. Shankar PM, Krishna PD, Newhouse VL. Subharmonic backscattering from ultrasound contrast agents. Journal of the Acoustical Society of America. 1999; 106(4):2104–10. [PubMed: 10530033]

8. Daeichin V, Bosch JG, Needles A, et al. Subharmonic, non-linear fundamental and ultraharmonic imaging of microbubble contrast at high frequencies. Ultrasound in Medicine and Biology. 2015; 41(2):486–97. [PubMed: 25592458]

9. Shi WT, Forsberg F, Raichlen JS, Needleman L, Goldberg BB. Pressure dependence of subharmonic signals from contrast microbubbles. Ultrasound in Medicine and Biology. 1999; 25(2):275–83. [PubMed: 10320317]

10. Halldorsdottir VG, Dave JK, Leodore LM, et al. Subharmonic Contrast Microbubble Signals for Noninvasive Pressure Estimation under Static and Dynamic Flow Conditions. Ultrasonic Imaging. 2011; 33(3):153–64. [PubMed: 21842580]

11. Shi WT, Forsberg F, Hall AL, et al. Subharmonic imaging with microbubble contrast agents: Initial results. Ultrasonic Imaging. 1999; 21(2):79–94. [PubMed: 10485563]

12. Forsberg F, Shi WT, Goldberg BB. Subharmonic imaging of contrast agents. Ultrasonics. 2000; 38(1-8):93–8. [PubMed: 10829636]

13. Chomas J, Dayton P, May D, Ferrara K. Nondestructive subharmonic imaging. Ieee Transactions on Ultrasonics Ferroelectrics and Frequency Control. 2002; 49(7):883–92.

14. Faez T, Emmer M, Docter M, et al. Characterizing the subharmonic response of phospholipid-coated microbubbles for carotid imaging. Ultrasound in Medicine and Biology. 2011; 37(6):958–70. [PubMed: 21531498]

15. Goertz DE, Cherin E, Needles A, et al. High frequency nonlinear B-scan imaging of microbubble contrast agents. Ieee Transactions on Ultrasonics Ferroelectrics and Frequency Control. 2005; 52(1):65–79.

16. Dave JK, Halldorsdottir VG, Eisenbrey JR, et al. Investigating the efficacy of subharmonic aided pressure estimation for portal vein pressures and portal hypertension monitoring. Ultrasound in Medicine and Biology. 2012; 38(10):1784–98. [PubMed: 22920550]

17. Eisenbrey JR, Dave JK, Halldorsdottir VG, et al. Chronic Liver Disease: Noninvasive Subharmonic Aided Pressure Estimation of Hepatic Venous Pressure Gradient. Radiology. 2013; 268(2):581–8. [PubMed: 23525208]

18. Biagi E, Breschi L, Varmacci E, Masotti L. Subharmonic emissions from microbubbles: Effect of the driving pulse shape. Ieee Transactions on Ultrasonics Ferroelectrics and Frequency Control. 2006; 53(11):2174–82.

19. Shekhar H, Doyley MM. Improving the sensitivity of high-frequency subharmonic imaging with coded excitation: A feasibility study. Medical Physics. 2012; 39(4):2049–60. [PubMed: 22482626]

20. Dave JK, Halldorsdottir VG, Eisenbrey JR, et al. On the implementation of an automated acoustic output optimization algorithm for subharmonic aided pressure estimation. Ultrasonics. 2013; 53(4):880–8. [PubMed: 23347593]

21. Dave JK, Halldorsdottir VG, Eisenbrey JR, et al. Noninvasive Estimation of Dynamic Pressures In Vitro and In Vivo Using the Subharmonic Response From Microbubbles. Ieee Transactions on Ultrasonics Ferroelectrics and Frequency Control. 2011; 58(10):2056–66.

22. Dave JK, Halldorsdottir VG, Eisenbrey JR, et al. Subharmonic microbubble emissions for noninvasively tracking right ventricular pressures. American Journal of Physiology-Heart and Circulatory Physiology. 2012; 303(1):H126–H32. [PubMed: 22561300]

23. Dave JK, Halldorsdottir VG, Eisenbrey JR, et al. Noninvasive LV Pressure Estimation Using Subharmonic Emissions From Microbubbles. Jacc-Cardiovascular Imaging. 2012; 5(1):87–92. [PubMed: 22239898]

24. Dave JK, Liu J-B, Halldorsdottir VG, et al. Acute Portal Hypertension Models in Dogs Low- and High-Flow Approaches. Comparative Medicine. 2012; 62(5):419–26. [PubMed: 23114046]

25. Eisenbrey JR, Dave JK, Halldorsdottir VG, et al. Simultaneous grayscale and subharmonic ultrasound imaging on a modified commercial scanner. Ultrasonics. 2011; 51(8):890–7. [PubMed: 21621239]

26. Pinnock C. Wylie and Churchill-Davidson's A Practice of Anesthesia: British journal of anaesthesia. 2004

27. Halpern EJ, mccue PA, Aksnes AK, et al. Contrast-enhanced US of the prostate with sonazoid: Comparison with whole-mount prostatectomy specimens in 12 patients. Radiology. 2002; 222(2): 361–6. [PubMed: 11818600]

28. Maresca D, Jansen K, Renaud G, et al. Intravascular ultrasound chirp imaging. Applied Physics Letters. 2012; 100(4)

29. Daeichin V, Faez T, Renaud G, et al. Effect of self-demodulation on the subharmonic response of contrast agent microbubbles. Physics in Medicine and Biology. 2012; 57(12):3675–91. [PubMed: 22614693]
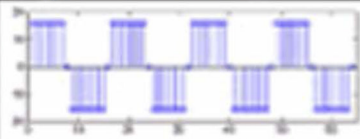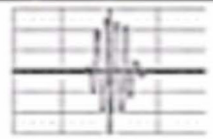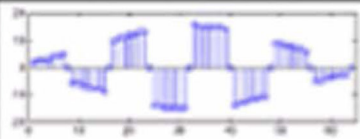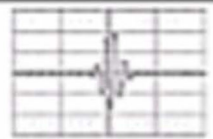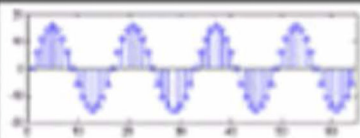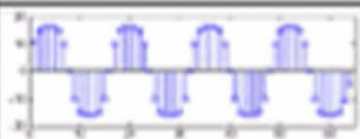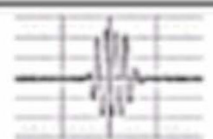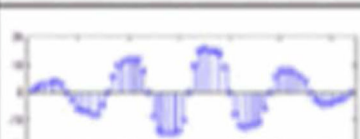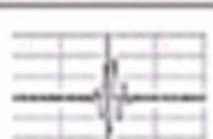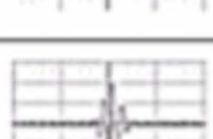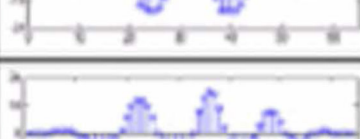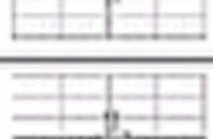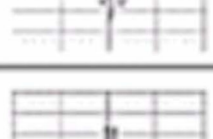
	Description	Input Waveform	Hydrophone
A	Square Wave		
B	Gaussian Windowed Square Wave		
C	Sine Wave		
D	Binomial Filtered Square Wave		
E	Gaussian Windowed Binomial Filtered Square		
F	Gaussian Windowed Binomial Filtered Square 90° shift		
G	Chirp Up		
H	Chirp Down		

Figure 1.
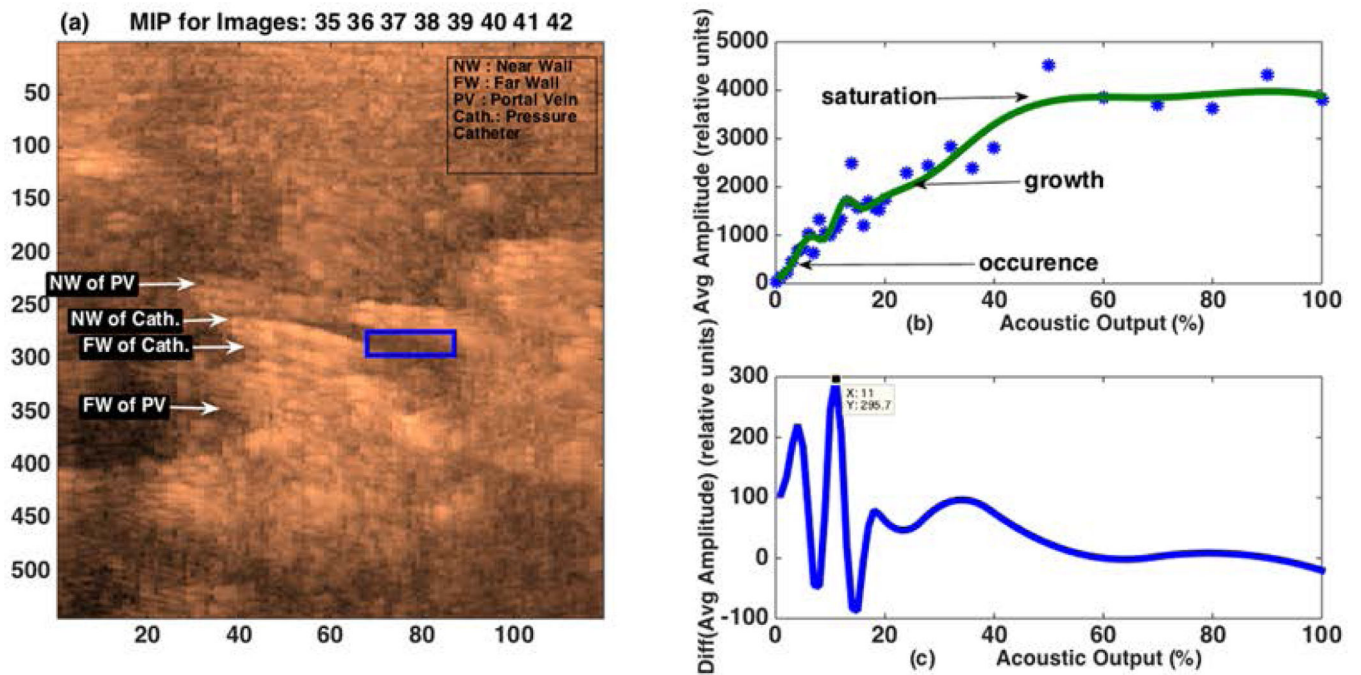Waveform settings implemented for SHI and SHAPE investigation

Figure 2.
Automated power optimization algorithm, [a]: Maximum Intensity Projection of SHI, blue square represents the region of interest selected within the portal vein; [b]: the three stages of subharmonic signal generation namely occurrence, growth and saturation with changing incident pressures from 0 to 100% of maximum acoustic pressures,[c]: y axis represents the change in subharmonic amplitude mapped from the top figure, the point represented by the highest peak is shown to have the highest SHAPE sensitivity
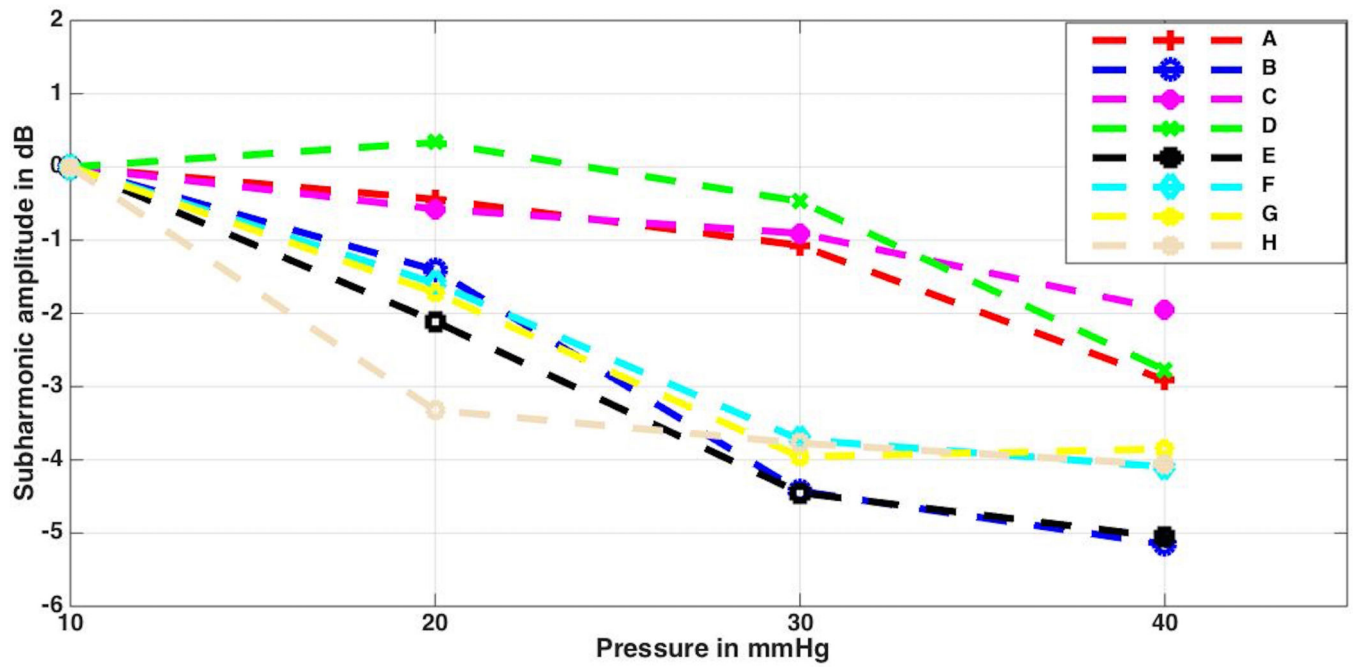
Figure 3.

In vitro setup : The relation between the mean subharmonic amplitude and the pressure for all eight pulse envelope in the in vitro setup. Each data point is the average of three readings taken at each pressure value for each waveform i.e., a total of 12 subharmonic amplitude values for each waveform
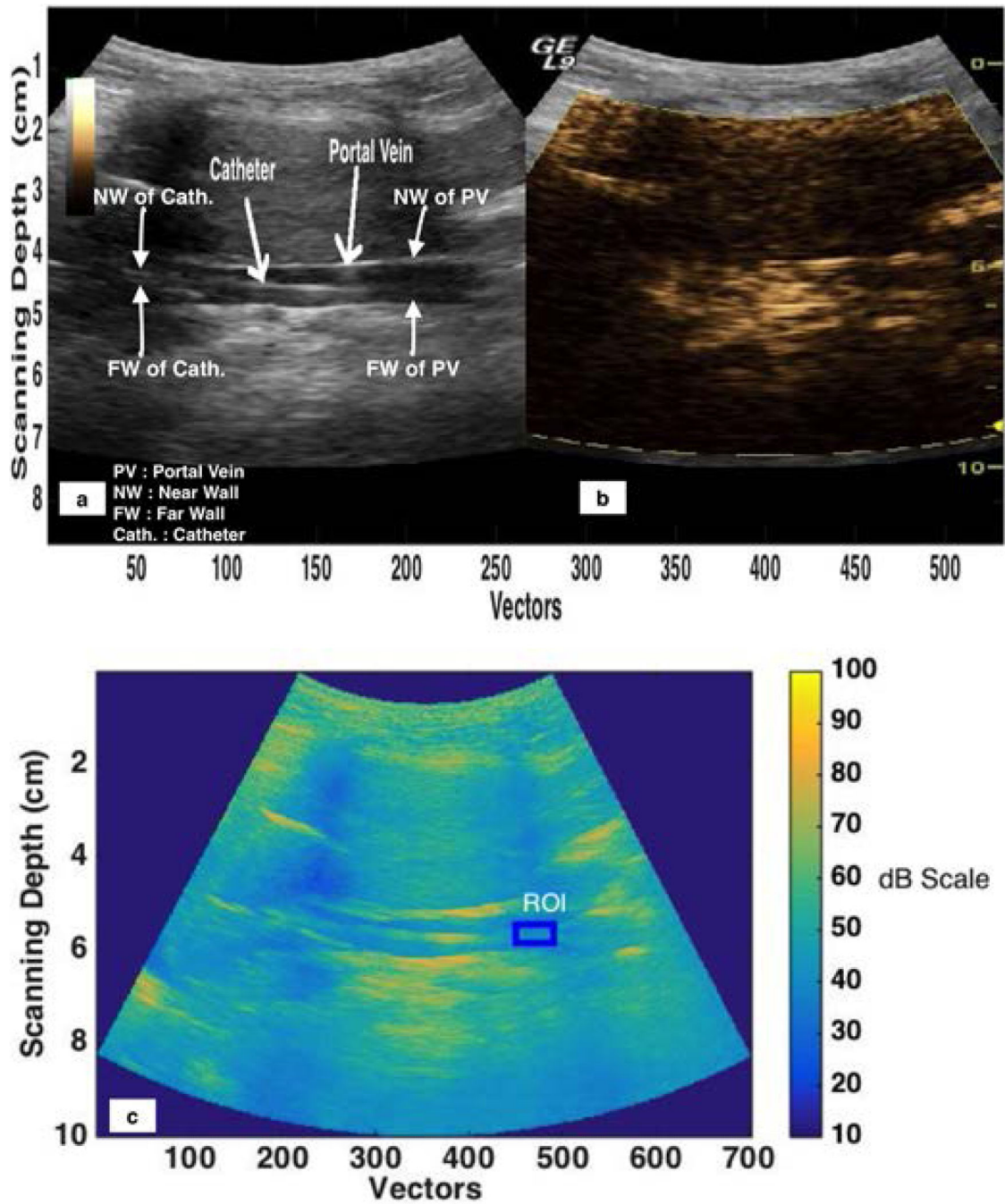
Figure 4.
[a] Dual Imaging with B mode(black and white) and SHI (b) on the left and right respectively;[c] region of interest selection on the Maximum Intensity Projection of the B mode Image

Table 1

Slope (between the subharmonic amplitude and ambient pressure ; normalized using log transform) and r values for all eight waveforms (A-H) *in vitro*

	A	B	C	D	E	F	G	H
SLOPE(dB/mmHg)	−0.10	−0.17	−0.06	−0.09	−0.17	−0.14	−0.13	−0.14
r	−0.88	−0.90	−0.79	−0.77	−0.95	−0.93	−0.91	−0.81

Table 2

Slope (between the subharmonic amplitude and ambient pressure ; normalized using log transform) and r values for all eight waveforms (A-H) for both canines

Waveform	Canine 1		Canine 2	
	Slope(dB/mmHg)	r values	Slope(dB/mmHg)	r values
A	−0.25	−0.91	−0.01	0
B	−0.37	−0.84	−0.26	−0.92
C	−0.32	−0.91	−0.16	−0.85
D	−0.33	−0.92	−0.2	−0.98
E	−0.44	−0.95	−0.46	−0.96
F	−0.2	−0.98	−0.28	−0.85
G	−0.28	−0.72	−0.49	−0.94
H	−0.33	−0.96	−0.51	−0.92